HHS Public Access

Author manuscript

Cell Host Microbe. Author manuscript; available in PMC 2019 July 11.

Published in final edited form as:

Cell Host Microbe. 2018 July 11; 24(1): 120–132.e6. doi:10.1016/j.chom.2018.06.002.

The Stringent Response Determines the Ability of a Commensal Bacterium to Survive Starvation and to Persist in the Gut

Whitman B. Schofield[1,2,3], **Maria Zimmermann-Kogadeeva**[1,2], **Michael Zimmermann**[1], **Natasha A. Barry**[1], and **Andrew L. Goodman**[1,4,*]

[1]Department of Microbial Pathogenesis and Microbial Sciences Institute, Yale University School of Medicine, New Haven, CT 06536, USA

SUMMARY

In the mammalian gut, bacteria compete for resources to maintain their populations, but the factors determining their success are poorly understood. We report that the human gut bacterium Bacteroides thetaiotaomicron relies on the stringent response, an intracellular signaling pathway that allocates resources away from growth, to survive carbon starvation and persist in the gut. Genome-scale transcriptomics, ^{13}C-labeling, and metabolomics analyses reveal that B. thetaiotaomicron uses the alarmone (p)ppGpp to repress multiple biosynthetic pathways and upregulate tricarboxylic acid (TCA) cycle genes in these conditions. During carbon starvation, (p)ppGpp triggers accumulation of the metabolite alpha-ketoglutarate, which itself acts as a metabolic regulator; alpha-ketoglutarate supplementation restores viability to a (p)ppGpp-deficient strain. These studies uncover how commensal bacteria adapt to the gut by modulating central metabolism and reveal that halting rather than accelerating growth can be a determining factor for membership in the gut microbiome.

In Brief

Schofield and Zimmermann-Kogadeeva et al. establish that B. thetaiotaomicron relies on (p)ppGpp signaling to halt growth, allowing this commensal to survive carbon starvation and persist in the gut. (p)ppGpp increases α-ketoglutarate, which alters metabolic processes that promote survival. Thus, halting growth is a requirement for membership in the gut microbiome.

*Correspondence: andrew.goodman@yale.edu.

[2]These authors contributed equally

[3]Present address: Department of Immunobiology, Yale University School of Medicine, New Haven, CT 06520, USA

[4]Lead Contact

SUPPLEMENTAL INFORMATION

Supplemental Information includes five figures and seven tables and can be found with this article online at https://doi.org/10.1016/j.chom.2018.06.002.

DECLARATION ON INTERESTS

The authors declare no competing interests.

AUTHOR CONTRIBUTIONS

Conceptualization: W.B.S., M.Z.-K., A.L.G.; Methodology: W.B.S., M.Z.-K., M.Z., N.A.B., A.L.G.; Formal analysis: M.Z.-K., W.B.S.; Investigation: W.B.S., M.Z.-K., M.Z., N.A.B.; Data curation: M.Z.-K., W.B.S.; Writing – Original Draft: M.Z.-K., W.B.S., A.L.G.; Writing – Review & Editing: M.Z.-K., W.B.S., M.Z., A.L.G.; Visualization: M.Z.-K., W.B.S.; Supervision: A.L.G.; Funding Acquisition: A.L.G., M.Z., M.Z.-K.

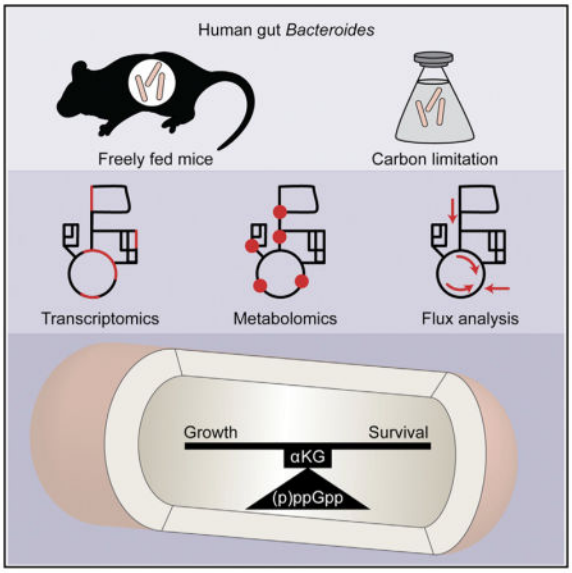

INTRODUCTION

Variation in gut microbiome composition has wide-ranging implications for health, and understanding the factors that shape community composition in this environment would enable efforts to restore or reshape these bacterial communities. In the healthy distal gut, resident bacteria (largely Bacteroidetes and Firmicutes) maintain populations exceeding 10^{11} cells per milliliter despite constant peristalsis, high bacteriophage levels, immune surveillance, and other challenges. Half of the microbial cells in fecal samples are dead or damaged (Bojanova and Bordenstein, 2016; Maurice et al., 2013), further increasing the burden on active cells to replicate at rates sufficient to maintain these populations. Prominent gut commensals, such as the Bacteroidetes, dedicate 20% of their genomes to machineries that extract carbon and other biomass precursors from available polysaccharides (Fischbach and Sonnenburg, 2011; Koropatkin et al., 2012). Transcriptome profiling and fluorescence dilution studies are also consistent with rapid bacterial growth in the gut (Myhrvold et al., 2015; Sonnenburg et al., 2005). Notably, many bacteria have also evolved mechanisms to arrest growth, but whether such pathways play a role in the microbial ecology of the gut is unknown.

Bacteria adapt their physiology from growth to survival by producing two intracellular alarmones, guanosine-5′-3′-bispyrophosphate (ppGpp) and guanosine pentaphosphate (pppGpp) (Cashel et al., 1996). In *Escherichia coli*, these signaling molecules interact with RNA polymerase to alter the expression of hundreds of genes in response to amino acid starvation (Ross et al., 2013) and other stresses, including limitation for carbon, nitrogen, fatty acids, iron, and phosphate (Boutte and Crosson, 2013; Potrykus and Cashel, 2008). Other bacteria use (p)ppGpp signaling in response to stresses specific to their environment (for example, non-optimal CO_2 or O_2 levels) in order to shift from growth to stasis or to induce sporulation (Braeken et al., 2006). Multiple pathogens couple (p)ppGpp signaling to virulence factor production (Dalebroux et al., 2010; Hauryliuk et al., 2015). In addition to

interactions with RNA polymerase (Lemke et al., 2009; Ross et al., 2013), the regulatory repertoire employed by (p)ppGpp spans a broad range of direct and indirect mechanisms (Dalebroux and Swanson, 2012; Gaca et al., 2015; Liu et al., 2015), including interaction with a variety of other proteins (Kanjee et al., 2012), σ-factor competition (Jishage et al., 2002), or modulation of the levels of initiating nucleoside triphosphates, such as guanosine triphosphate (GTP) (Krásný and Gourse, 2004).

The cellular pool of (p)ppGpp is controlled by Rel-Spo Homolog (RSH) proteins. Most bacteria encode a single RSH protein that contains both (p)ppGpp synthetase and hydrolase domains, while Beta- and Gammaproteobacteria, including *E. coli*, have duplicated RSH genes (Potrykus and Cashel, 2008). In these species, one RSH homolog (RelA in *E. coli*) carries inactivating mutations in the hydrolase domain, while the other (SpoT in *E. coli*) retains both (p)ppGpp synthetase and hydrolase activity (Figure 1A). Because unrestrained (p)ppGpp production inhibits growth, SpoT is essential if RelA is present (Xiao et al., 1991).

In the course of identifying candidate essential genes by genomewide transposon mutagenesis of the human gut commensal *Bacteroides thetaiotaomicron* (Goodman et al., 2009), we noticed that one of two predicted RSH genes (*bt3998*) was completely recalcitrant to transposon insertion. Because (p)ppGpp production is not essential for viability in other organisms, and *B. thetaiotaomicron* encodes a second RSH enzyme, we reasoned that *bt3998*-dependent (p)ppGpp hydrolase activity could be required for viability in this organism. In this work, we set out to investigate the contribution of the (p)ppGpp alarmones in a representative human gut commensal.

Here we report that (p)ppGpp signaling plays a critical role in determining the ability of *B. thetaiotaomicron* to colonize and persist in the gut of freely fed mice. Moreover, (p)ppGpp regulation ensures *B. thetaiotaomicron* survival during carbon starvation *in vitro*. RNA sequencing (RNA-seq) analysis defines a common (p)ppGpp-dependent central metabolism gene expression program that *B. thetaiotaomicron* activates in these two conditions. Metabolomics and ^{13}C-tracing experiments reveal that (p)ppGpp production triggers significant increases in the levels of succinate and alpha-ketoglutarate (AKG) upon carbon starvation. Notably, AKG supplementation rescues the starvation survival defect of a ppGpp^0 strain. Together, these studies provide an example of a human gut commensal that relies on intracellular signals that halt growth in favor of starvation survival in order to persist in the gut of a non-starved host.

RESULTS

Bacteroides thetaiotaomicron Encodes Two (p)ppGpp Synthases Required for Carbon Starvation Survival but Dispensable for Amino Acid Biosynthesis

Human gut *Bacteroides* encode two multi-domain RSH enzymes (represented by BT0700 and BT3998 in *B. thetaiotaomicron*) that have not been functionally characterized. These enzymes share greater sequence similarity with each other than either does to RelA or SpoT from Gammaproteobacteria, suggesting that RSH gene duplication events occurred independently in both the Bacteroidetes and Gammaproteobacteria lineages (Figure 1B) (Atkinson et al., 2011). Three lines of evidence suggest that BT0700 and its homologs, like

E. coli RelA, have lost (p)ppGpp hydrolase activity. First, half of the amino acid positions that are required for hydrolase activity in homologous proteins (Hogg et al., 2004) are altered to functionally dissimilar amino acids in BT0700 and its homologs in *Bacteroides ovatus, Bacteroides eggerthii, Bacteroides uniformis,* and *Bacteroides vulgatus* (Figure 1B, Table S1). By contrast, the hydrolase domain in BT3998 and its homologs contain functionally dissimilar amino acids in few of these positions. Second, random transposon mutagenesis of each of these species yields numerous insertions in the *bt0700* homolog, but none in the *bt3998* homolog encoded in each species (Figure S1A) (Cullen et al., 2015), consistent with previous assignment of *bt3998* as a candidate essential gene (Goodman et al., 2009). Third, *bt3998* is readily deleted in the *bt0700* background, but not in the wild-type background (Table S2).

To determine whether BT0700 and BT3998 are indeed required for (p)ppGpp synthesis, we analyzed ^{32}P-labeled nucleotide extracts from wild-type and mutant strains by thin-layer chromatography. In response to carbon starvation, wild-type *B. thetaiotaomicron* increases the levels of two characteristic nucleotides that migrate between GTP and the origin. The levels of these nucleotides are reduced in the *bt0700* strain and not detected in the *bt0700 bt3998* strain (Figure 1C). Quantification of (p)ppGpp levels relative to GTP reveals that during carbon starvation, the wild-type strain accumulates three times more alarmone than the *bt0700* mutant (Figure S1B). Detection of ppGpp prior to carbon starvation in ^{32}P-labeled wild-type cells likely results from minor oxygen exposure, which induces alarmone production in *B. thetaiotaomicron* (Glass et al., 1979). Liquid chromatography-coupled massspectrometry (LC-qTOF) quantification confirms production of ppGpp upon carbon starvation (Figure S1C). Based on these results, we designated the *bt0700 bt3998* strain as ppGpp^0.

Since carbon starvation activates (p)ppGpp production by *B. thetaiotaomicron*, we next determined whether this signal is important for survival in this condition. Indeed, wild-type *B. thetaiotaomicron* readily withstands 24 hr of carbon starvation with no significant loss of viability; by contrast, the viability of the ppGpp^0 strain decreases by four orders of magnitude (Figure 1D). Since deletion of *bt0700* decreases viability only 2-fold at the same time point (Table S3), we conclude that (p)ppGpp produced by BT3998 is largely sufficient to maintain cellular survival during 24 hr of carbon starvation.

In many bacteria, (p)ppGpp signaling is essential for activation of amino acid biosynthetic pathways in the absence of exogenous amino acids; as a result, ppGpp^0 strains are auxotrophic for multiple amino acids (Hauryliuk et al., 2015). Notably, the *B. thetaiotaomicron* ppGpp^0 strain readily grows in defined amino acid-free minimal medium (Figure 1E). Although the ppGpp^0 growth rate is 20% slower than the wild-type, amino acid supplementation increases both growth rates to an equivalent extent (Figure 1F). Together, these results suggest that (p)ppGpp signaling is essential for carbon starvation survival, but not amino acid biosynthesis, in *B. thetaiotaomicron*.

B. thetaiotaomicron Requires (p)ppGpp for Establishment and Maintenance of Gut Colonization

To assess the role of (p)ppGpp signaling in mammalian gut colonization, we conducted three experiments in gnotobiotic mice. First, we colonized germfree mice fed nutrient-rich chow *ad libitum* with a combination of *B. thetaiotaomicron* wild-type, *bt0700,* and ppGpp^0 strains (1:10:10), and measured population dynamics over time in fecal samples. Within 8 days of initial colonization, the ppGpp^0 strain is outcompeted by six orders of magnitude (Figure 2A). The *bt0700* strain exhibits a transient decrease in competitive fitness, which is no longer apparent by day 15 (Figures 2A and S2, Table S3). There is no difference in the colonization levels of wild-type, *bt0700,* and ppGpp^0 strains when introduced individually into separate mice (Figure 2B).

Second, to determine whether (p)ppGpp signaling is also required in the presence of other abundant members of the human gut microbiota, we colonized gnotobiotic mice with the *B. thetaiotaomicron* wild-type, *bt0700*, and ppGpp^0 strains together with six human gut Bacteroidetes or six prominent human gut Firmicutes and Actinobacteria (STAR Methods). In each of these defined communities, the *B. thetaiotaomicron* ppGpp^0 strain demonstrates an equivalent fitness defect as observed in the absence of other species (Figure 2C).

Bacteroides species exhibit intraspecific niche exclusion in the gut, in which initial colonizers prevent subsequent establishment by the same species (Lee et al., 2013). In the third experiment, we colonized germfree mice with barcoded wild-type (WT^A) or ppGpp^0 *B. thetaiotaomicron* strains; after 3 days, we introduced a differently barcoded wild-type strain (WT^B), and measured population dynamics over time (Figure 2D). As expected, the WT^A strain efficiently prevented WT^B colonization. By contrast, the ppGpp^0 strain was unable to exclude the WT^B strain, suggesting that (p)ppGpp signaling provides a fitness advantage both for initial colonization and long-term persistence in the gut.

B. thetaiotaomicron Maintains a Common (p)ppGpp-Dependent Metabolic Gene Expression Program *In Vivo* and during Carbon Starvation *In Vitro*

To identify (p)ppGpp-dependent processes that determine *B. thetaiotaomicron* fitness, we performed RNA-seq analysis of wild-type, *bt0700*, and ppGpp^0 strains during growth *in vitro* before and after 1 hr of carbon starvation and *in vivo* in cecal contents of monocolonized gnotobiotic mice. Overall, nearly 60% of the transcriptome is differentially expressed between the wild-type and ppGpp^0 strains in at least one condition (Table S4), reflecting a broad transcriptional program that responds to the (p)ppGpp signal.

Principal component analysis (PCA) of the normalized RNA-seq data separates transcriptional profiles by experimental condition, suggesting that environment plays the largest role in defining the observed transcriptional profiles (Figure 3A). When PCA is applied separately to *in vitro* and *in vivo* data, the first principal component separates ppGpp^0 from the wild-type and *bt0700* strains *in vivo* and during starvation *in vitro*, implying that (p)ppGpp-dependent gene regulation has a broad effect in these conditions (Figures 3B and 3C).

To survey the processes affected by (p)ppGpp deficiency, we performed pathway enrichment analysis to identify Kyoto Encyclopedia of Genes and Genomes (KEGG) pathways (Ogata et al., 1999) enriched in differentially expressed genes between $ppGpp^0$ and wild-type strains in each condition ($|\log_2[\text{fold change}]| \geq 1$, false discovery rate [FDR] ≤0.05). The majority of pathways enriched in downregulated genes in the $ppGpp^0$ strain are condition-independent, and few pathways are enriched in $ppGpp^0$-upregulated genes during *in vitro* growth (Figure 3D, Table S4). During both carbon starvation and gut colonization, pathways associated with metabolism of various amino acids, folate, and biotin, aminoacyl-tRNA biosynthesis, and ABC transporters are enriched in upregulated genes in the $ppGpp^0$ strain (Figure 3D). These results further indicate that *B. thetaiotaomicron* uses (p)ppGpp signaling to control shared processes in these different environments.

Because the wild-type and *bt0700* strains both exhibit a significant fitness advantage over the $ppGpp^0$ strain during gut colonization (Figure 2A), we reasoned that the gene regulatory events that determine *in vivo* fitness are likely shared between wild-type and *bt0700* strains, and distinct between either of these strains and the $ppGpp^0$ strain. Pathway enrichment analysis highlights folate, polyketide sugar unit, and aliphatic amino acid biosynthesis pathways enriched in $ppGpp^0$-upregulated genes; and tricarboxylic acid (TCA) cycle and alanine/aspartate/glutamate metabolism pathways enriched in $ppGpp^0$-downregulated genes as compared with both wild-type and *bt0700* strains (Figure 3E). Several pathways are enriched in both upregulated and downregulated genes, suggesting that parts of these pathways may fulfill different functions and undergo different regulatory programs.

To characterize these $ppGpp^0$-specific differences independent from pathway definitions, we selected the differentially expressed genes in the $ppGpp^0$ compared with both the wild-type and *bt0700* strains *in vivo,* and performed a metabolic subnetwork analysis (Zimmermann et al., 2017). We mapped these 395 genes onto a network generated from KEGG reaction pairs (Ogata et al., 1999) representing substrate and product metabolites as nodes, connected by enzymes (edges). We then used a shortest path search algorithm to identify subnetworks consisting of at least three connected genes regulated in a (p)ppGpp-specific manner. We detected five such subnetworks that cover central metabolism (glycolysis, pentose phosphate pathway, and TCA cycle), amino acid metabolism, polyketide sugar unit biosynthesis, starch and sucrose metabolism, and lipoic acid metabolism (Figure 3F, Table S4). Notably, these *in vivo* (p)ppGpp-regulated metabolic subnetworks exhibit the same expression pattern during carbon starvation *in vitro* (Figure 3G, Table S4). Concordant with the KEGG pathway enrichment analysis, subnetworks associated with amino acid metabolism are repressed in a (p)ppGpp-dependent manner, while subnetworks associated with central metabolism require (p)ppGpp for upregulation, both *in vivo* and *in vitro* during starvation.

Carbon Starvation Induces (p)ppGpp-Dependent Changes in TCA Cycle Gene Expression and TCA Cycle Metabolites

Since transcriptional analysis revealed (p)ppGpp-dependent regulation of numerous metabolic pathways, we set out to investigate stress-induced metabolic adaptations by directly measuring intracellular metabolites. Given the difficulty of distinguishing bacterial and host central metabolites *in vivo*, and the high similarity between (p)ppGpp-dependent

transcriptional responses in the gut and during carbon starvation (Figures 3F and 3G), we focused on wild-type and ppGpp^0 *B. thetaiotaomicron* cultures collected before and 1 hr after carbon starvation. At this time point, the ppGpp^0 strain does not yet exhibit a significant loss of viability (Figure 1D, Table S3).

Transcriptional changes induced by carbon starvation fall into three categories: KEGG pathways enriched in upregulated genes by both strains, in downregulated genes by both strains, and in genes downregulated only by the wild-type strain (Figure S3A, Table S4). Glycan and lipid degradation, as well as galactose, histidine, and pentose metabolism pathways were upregulated, whereas glycolysis, several amino acids, propanoate, and ribosome pathways were downregulated in a (p)ppGpp-independent manner. Numerous pathways involved in amino acid, purine and pyrimidine, peptidoglycan, folate, biotin, and aminoacyl-tRNA biosynthesis, as well as RNA polymerase and RNA degradation, were downregulated only by the wild-type strain, consistent with an inability of the (p)ppGpp-deficient strain to inhibit growth upon starvation. Transcriptional changes in the *bt0700* strain resembled those of the wild-type (Figure S3A), suggesting that (p)ppGpp it produces (Figure 1C) is sufficient to induce the response to carbon starvation.

Because (p)ppGpp signaling impacts expression of many metabolic genes *in vivo* and during starvation, we next measured metabolites directly by untargeted metabolomics analysis of wild-type and ppGpp^0 samples. We detected 2,512 ions shared between the growth and starvation conditions, 176 of which could be annotated and assigned to 70 out of 77 KEGG metabolic pathways in *B. thetaiotaomicron* (Table S5). Pathway enrichment analysis of significantly changing metabolites between the 1-hr carbon starvation and carbon-replete conditions in the wild-type and ppGpp^0 strains ($|\log_2[\text{fold change}]| \geq \log_2[1.5]$, FDR ≤ 0.05) reveals heterogeneous changes, with many pathways being enriched in both decreasing and increasing metabolites (Figure 4A). Similar to the transcriptional response, the ppGpp^0 strain fails to decrease metabolites in amino acid and aminoacyl-tRNA biosynthesis pathways. Furthermore, ppGpp^0 fails to increase metabolites associated with amino acid, butanoate, glyoxylate metabolism, and TCA cycle pathways (Figure 4A, Table S5).

We next used targeted metabolite measurements (liquid chromatography coupled tandem mass spectrometry [LC-MS/MS]) to selectively quantify the levels of 30 metabolites associated with central, amino acid, and nucleoside metabolism. Consistent with the role of GTP as the precursor of pppGpp (Figure 1A) (Krásný and Gourse, 2004), guanosine diphosphate (GDP) and GTP levels decrease in wild-type *B. thetaiotaomicron* but not in the ppGpp^0 strain upon carbon starvation (Figure 4B). Whereas both the wild-type and ppGpp^0 strains decrease glycolysis and pentose phosphate pathway intermediates upon starvation, the TCA cycle metabolites succinate and alpha-ketoglutarate (AKG) are highly and specifically increased in a (p)ppGpp-dependent manner when the carbon source is withdrawn (Figure 4B, Table S5). Concurrently, the wild-type strain upregulates several TCA cycle genes, while the ppGpp^0 strain fails to do so (Figures 4C and 4D, Table S4). We therefore hypothesized that these (p)ppGpp-dependent differences in succinate and AKG levels contribute to the stress response program. We set out to further investigate the source of these accumulating TCA cycle metabolites and their effect on bacterial survival during carbon starvation.

B. thetaiotaomicron Produces Alpha-Ketoglutarate via the Reductive Branch of the TCA Cycle during Growth and Starvation

To investigate succinate and AKG production in *B. thetaiotaomicron*, we first analyzed TCA cycle operation in *B. thetaiotaomicron* during growth in glucose minimal medium. To this end, we shifted exponentially growing wild-type *B. thetaiotaomicron* from [U-^{12}C]-glucose to labeled [U-^{13}C]-glucose on a filter under continual culture medium flow, and measured mass isotopologues of intracellular metabolites over the course of 5 minutes by LC-MS/MS as described (Link et al., 2013) (Figure S4A). The metabolite labeling patterns reflect ^{13}C propagation from [U-^{13}C]-glucose and $^{12}CO_2$ integration from the anaerobic atmosphere, which contains 20% CO_2.

After exponentially growing *B. thetaiotaomicron* cultures are shifted to [U-^{13}C]-glucose, the label rapidly propagates through glycolysis, with its intermediates fructose-bisphosphate (FBP) and phosphoenolpyruvate (PEP) reaching the labeled isotopic steady state within 160 s. Labeling steady state is nearly reached in malate and succinate in the reductive branch, and not reached in citrate in the oxidative branch of the TCA cycle within this time (Figure 5A). The labeling pattern of glutamate matches that of succinate and not citrate, suggesting that glutamate and its immediate precursor AKG are produced via the reductive TCA cycle (Figures 5A and 5E). Consistent with these observations, providing growing cells with [U-^{13}C]-acetate (metabolized in the first step of the oxidative branch) results in label propagation to citrate, but not glutamate (Figures 5B and 5E, Table S6).

We next took two approaches to investigate TCA cycle operation during carbon starvation. Because *B. thetaiotaomicron* is unable to grow on acetate or glutamine as a sole carbon source (Figure S4B), we shifted cells from medium containing unlabeled glucose and either [U-^{13}C] acetate or [U-^{12}C] glutamine to medium lacking glucose and containing either [U-^{13}C]-acetate or [U-^{13}C] glutamine to probe the fluxes to AKG through the oxidative TCA cycle and from amino acids. During the acetate shift, the ^{13}C label propagates to citrate but not to glutamate or other measured metabolites, suggesting that AKG is not produced from the oxidative branch (Figures 5C and 5E). In the presence of [U-^{13}C]-glutamine, the label was detected only in glutamate (Figure 5D). Since we could not directly measure the AKG labeling pattern, we cannot exclude that some label from citrate or glutamate propagates to AKG, but not further. Parallel experiments conducted with the ppGpp^0 mutant revealed similar patterns in label propagation in intracellular metabolites (Figures S4C and S4D). Together, these studies establish that both wild-type and ppGpp^0 strains of *B. thetaiotaomicron* operate a bifurcated TCA cycle, with AKG and glutamate derived from succinate via the reductive branch. Our data suggest that during carbon starvation, the reductive branch remains the major source of increased AKG, despite the upregulation of the oxidative branch enzymes.

Supplementation with Alpha-Ketoglutarate Enhances ppGpp^0 Survival during Carbon Starvation

Our transcriptomic and metabolomic analyses point out the engagement of the TCA cycle in the (p)ppGpp-dependent global regulatory program in *B. thetaiotaomicron*. To determine whether the failure of the ppGpp^0 strain to modulate the TCA cycle contributes to its lack of

fitness, we focused on AKG, which is highly increased upon starvation in a (p)ppGpp-dependent manner (Figures 4B–4D) and is derived from succinate (Figure 5). To this end, we treated ppGpp^0 cells with dimethyl-AKG (a membrane-permeable AKG precursor [Doucette et al., 2011]) 30 min prior and during carbon starvation. The intracellular levels of AKG, glutamate, and glutamine significantly increased, suggesting that dimethyl-AKG readily enters the cells and is hydrolyzed to AKG (Figures 6A and S5A). Strikingly, exogenous dimethyl-AKG protects the ppGpp^0 strain from its normal loss of viability during carbon starvation by nearly two orders of magnitude (Figure 6B, Table S3). It is unlikely that exogenous dimethyl-AKG rescues the ppGpp^0 strain by serving as a precursor for amino acids derived from glutamine, because addition of glutamine is not protective (Figure 6C). Further, it is unlikely that the protective effect of dimethyl-AKG can be explained by its replenishment of a carbon source, because its addition to growing *B. thetaiotaomicron* cultures results in growth arrest (Figure 6D).

To better understand how AKG protects *B. thetaiotaomicron* from loss of viability during starvation, we performed untargeted metabolomic profiling of the ppGpp^0 strain before and during carbon starvation, with and without dimethyl-AKG supplementation. Of 3,104 detected ions, 171 could be annotated and 68 had distinct dynamic profiles between the two conditions (Table S7). The large number of changing metabolites and the bidirectionality of changes suggest that AKG acts as a regulator, affecting pathways both proximal and distal from its entry point into the TCA cycle (Figure 6E, Table S7). Interestingly, dimethyl-AKG treatment does not prevent accumulation of GDP or other nucleotides in the ppGpp^0 strain (Figure S5B), suggesting that its protective effects are independent of guanosine nucleotide regulation.

Overall, our results suggest that upon starvation, *B. thetaiotaomicron* increases AKG levels in a (p)ppGpp-dependent manner. Elevated AKG, in turn, likely serves as a metabolic regulator and affects amino acid, pantothenate, propanoate, and central carbon metabolism, among others. An isogenic *B. thetaiotaomicron* strain genetically altered to lack (p)ppGpp signaling cannot increase AKG levels upon starvation and exhibits a severe viability defect under these conditions, which is substantially rescued by exogenous AKG supplementation.

DISCUSSION

The distal gut is a dynamic ecosystem, with enormous populations of bacteria competing for resources while facing rigorous immune surveillance, introduction of foreign microbes, and constant perfusion. Perhaps as a result, dominant gut microbes dedicate a large portion of their genomes to machineries that efficiently convert dietary polysaccharides into biomass for growth. These systems are well represented and best characterized in *B. thetaiotaomicron*, and transcriptomic studies in the gut of monoassociated gnotobiotic mice revealed that this species maintains a genomewide expression profile *in vivo* that is consistent with rapid growth (Sonnenburg et al., 2005). Here we report that *B. thetaiotaomicron* also relies on an intracellular signal to arrest growth in order to compete in the mammalian gut.

Genome-scale transcriptomics and metabolomics analyses uncover a broad (p)ppGpp-dependent metabolic response that *B. thetaiotaomicron* maintains in the gut. This (p)ppGpp-dependent gene expression program is also required to survive carbon starvation *in vitro*. In both conditions, *B. thetaiotaomicron* uses (p)ppGpp signaling to upregulate TCA cycle genes, and direct measurement of metabolite levels *in vitro* reveal a concordant, (p)ppGpp-dependent increase in TCA cycle metabolites. The TCA cycle intermediate AKG rescues the survival defect of a $ppGpp^0$ strain during starvation, highlighting this molecule as a key component of the (p)ppGpp regulatory repertoire.

(p)ppGpp as a Global Transcriptional Regulator in Starving *B. thetaiotaomicron*

B. thetaiotaomicron shares several general features of (p)ppGpp signaling observed in other bacterial phyla. As initially described in stringent strains of *E. coli*, *B. thetaiotaomicron* employs (p)ppGpp to repress rRNA and tRNA synthesis during starvation. Further, (p)ppGpp serves as a global regulator, altering the expression of more than 50% of the *B. thetaiotaomicron* genome during starvation (Table S4); this broad effect is also observed in other phyla (Potrykus and Cashel, 2008). This gene expression program extends beyond the transcription and translation apparatus to include (p)ppGpp-dependent repression of biosyntheticpathways for peptidoglycan, amino acids, and other metabolic pathways. Direct comparison of (p)ppGpp-mediated regulation with previous studies is hindered by differences in starvation conditions, since amino acid starvation is typically used to induce (p)ppGpp production in other bacteria (Eymann et al., 2002; Traxler et al., 2008), whereas *B. thetaiotaomicron* does not require (p)ppGpp to activate amino acid biosynthesis (Figures 1E and 1F). *Caulobacter crescentus,* another bacterium that does not require (p)ppGpp for activation of amino acid biosynthesis, exhibits similar (p)ppGpp-dependent downregulation of amino acid biosynthetic genes upon carbon starvation (Boutte and Crosson, 2011). Notably, the hourly time resolution of our studies does not differentiate between direct and secondary effects of (p)ppGpp regulation, both of which are likely important for its protective effects. Other aspects of *B. thetaiotaomicron* carbon starvation response are (p)ppGpp-independent, including upregulation of genes responsible for degrading glycans and lipids, and downregulation of genes associated with central metabolism (with the exception of the TCA cycle).

The Regulation of Starvation Response by Alpha-Ketoglutarate

In response to carbon starvation, *B. thetaiotaomicron* significantly upregulates TCA cycle gene expression in a (p)ppGpp-dependent manner and quadruples the levels of the TCA cycle metabolite AKG, which likely contributes to prolonged survival by promoting growth arrest. A regulatory role for AKG has been reported in Proteobacteria, where it coordinates carbon and nitrogen metabolism (Doucette et al., 2011) and peptidoglycan biosynthesis (Irnov et al., 2017). However, the proposed mechanism of AKG inhibition of glucose uptake in response to nitrogen starvation is unlikely to explain our observations, because *B. thetaiotaomicron* does not use the phosphotransferase system to transport glucose and is not nitrogen limited in these experiments; further, no glucose is present in the starvation condition. In *Caenorhabditis elegans,* AKG is reported to prolong lifespan through inhibition of ATP synthase (Chin et al., 2014). However, this mechanism is also unlikely to explain our results, since AKG supplementation does not change AMP or ADP levels in *B.*

thetaiotaomicron (Figure S5B). Dimethyl-AKG supplementation of the ppGpp^0 mutant at the onset of carbon starvation leads to a decrease in metabolic pathway intermediates which were decreased in the wild-type, but not in the unsupplemented ppGpp^0 strain (including metabolites associated with aminoacyl-tRNA biosynthesis, amino acid metabolism and biosynthesis pathways), and an increase in metabolic pathway intermediates increased in the wild-type but not in the ppGpp^0 strain (alanine, aspartate and glutamate, butanoate metabolism) (Figures 6E and 4A). We therefore hypothesize that AKG serves as a signal that coordinates the allocation of multiple resources away from biosynthesis pathways, and that the absence of this signal leads to rapid death during starvation.

The mechanisms by which (p)ppGpp stimulates AKG accumulation during starvation remain unclear. Although *B. thetaiotaomicron* induces expression of genes in the oxidative branch of the TCA cycle in a (p)ppGpp-dependent manner, no flux from citrate to AKG is detected during growth or starvation. TCA cycle bifurcation around succinate during anaerobic growth has been observed in other species (Amador-Noguez et al., 2010; Chen et al., 2011; Sauer et al., 1999). *Bacteroides fragilis* bifurcates the TCA cycle around AKG, which is produced either from succinate through the heme-dependent reductive branch, or from citrate through the heme-independent oxidative branch (Baughn and Malamy, 2002); however, their relative contributions have not been determined. Because *B. thetaiotaomicron* is auxotrophic for heme, we have not been able to investigate the contribution of the oxidative branch by eliminating heme. Notably, the oxidative branch of the TCA cycle is also upregulated during amino acid starvation in *E. coli* with concomitant increase of glutamate, a direct product of AKG, in a (p)ppGpp-dependent manner (Traxler et al., 2008). This suggests that the accumulation of AKG and related metabolites in response to stress is a conserved mechanism of (p)ppGpp-mediated regulation.

(p)ppGpp as an Essential Regulatory Mechanism for Gut Colonization

Our finding that *B. thetaiotaomicron* relies on the same intracellular signal to survive carbon starvation and to persist in the gut suggests that it faces significant and continual stresses in the gut environment, and that common physiological adaptations that favor stasis rather than growth are beneficial in both conditions. Although the mammalian gut provides a protected habitat of constant temperature and a continuous flow of nutrients that supports enormous bacterial populations, local environments encountered by bacteria are likely heterogeneous. The environmental cues that trigger (p)ppGpp-mediated stress responses in other bacteria vary between species (Boutte and Crosson, 2013). In Proteobacteria, RSH gene duplication further diversifies its stringent response, with RelA responding to single amino acid depletion (Haseltine and Block, 1973) and SpoT to fatty acid (Seyfzadeh et al., 1993), iron (Vinella et al., 2005), and carbon limitation. The *Bacteroides* lineage has also (independently) duplicated its ancestral RSH gene, although the spectrum and enzyme specificity of (p)ppGpp-inducing environmental cues remain undefined in these organisms.

In the gut, bacteria could be exposed to temporary nutrient and iron shortages, high or low oxygen and CO_2 levels, and high bacterial densities. The striking similarities between the transcriptional profiles of the *B. thetaiotaomicron* ppGpp^0 strain during *in vitro* carbon starvation and *in vivo* colonization suggest that carbon starvation might challenge bacteria in

the gut, even though the mice are fed *ad libitum*. In fact, the set of pathways differentially regulated between *in vitro* carbon-replete conditions and either carbon starvation or gut colonization are almost identical (Figures S3A and S3B). Pathways upregulated upon glucose removal *in vitro* and gut colonization (glycan degradation, sphingolipid metabolism, and others) are largely (p)ppGpp-independent, while (p)ppGpp primarily signals cells to stop growing by downregulating numerous biosynthetic pathways. The $ppGpp^0$ strain, which retains the ability to upregulate many of the same genes as the wild-type strain and adjust metabolite levels (with AKG as a notable exception) but lacks the ability to inhibit biosynthetic genes, rapidly loses viability during carbon starvation and exhibits a drastic fitness defect in the gut.

Several pathogenic bacteria require (p)ppGpp to colonize the lungs (Dahl et al., 2003; Kazmierczak et al., 2009) and intestines (Haralalka et al., 2003; Pizarro-Cerdá and Tedin, 2004), which has been mainly attributed to the inability of (p)ppGpp-deficient mutants to produce virulence factors. In addition to activating virulence factor production, (p)ppGpp is also associated with antibiotic resistance in diverse pathogens, making it an attractive drug target (Gaca et al., 2015). Indeed, several antibacterial agents have been reported to inhibit (p)ppGpp production and interfere with pathogenic infections (de la Fuente-Núñez et al., 2014; Wexselblatt et al., 2012). Our results suggest that molecules that inhibit (p)ppGpp might invoke an antibiotic rather than anti-virulence effect that could have a significant impact on the resident microbiota. Overall, we conclude that the ability to halt growth is a counter-intuitive but important requirement for intentional introduction of new members to the microbiome.

STAR★METHODS

Detailed methods are provided in the online version of this paper and include the following:

KEY RESOURCES TABLE

REAGENT or RESOURCE	SOURCE	IDENTIFIER
Bacterial and Virus Strains		
E. coli S17-1 lambda pir	ATCC	ATCC BAA-2428
B. thetaiotaomicron VPI-5482 tdk	PMID_18611383	N/A
B. thetaiotaomicron VPI-5482 tdk Δbt0700	This study	N/A
B. thetaiotaomicron VPI-5482 tdk Δbt0700Δbt3998	This study	N/A
B. thetaiotaomicron VPI-5482 tdk att1::pNBUBC21	This study	N/A
B. thetaiotaomicron VPI-5482 tdk Δbt0700 att1::pNBUBC14	This study	N/A
B. thetaiotaomicron VPI-5482 tdk Δbt0700Δbt3998 att1::pNBUBC22	This study	N/A
Bacteroides thetaiotaomicron VPI 5482	ATCC	ATCC 29148
Bacteroides vulgatus NCTC11154	ATCC	ATCC 8482
Bacteroides caccae VPI 3452A	ATCC	ATCC 43185
Bacteroides ovatus NCTC11153	ATCC	ATCC 8483
Bacteroides uniformis VPI 0061	ATCC	ATCC 8492
Prevotella copri 18205	DSM	DSM 18205
Parabacteroides distasonis	ATCC	ATCC 8503
Bifidobacterium adolescentis	DSM	DSM 20083
Collinsella aerofaciens VPI 1003	ATCC	ATCC 25986
Clostridium scindens VPI 13733	ATCC	ATCC 35704

REAGENT or RESOURCE	SOURCE	IDENTIFIER
Dorea longicatena 111-35	DSM	DSM 13814
Eubacterium rectale VPI 0990	ATCC	ATCC 33656
Blautia obeum VPI B3-21	ATCC	ATCC 29174
Chemicals, Peptides, and Recombinant Proteins		
Guanosine tetraphosphate, ppGpp	TriLink	Cat#N-6001
Phosphorus-32 Radionuclide, as dipotassium phosphate	PerkinElmer	Cat#NEX055002MC
PEI-cellulose TLC plates	Sigma-Aldrich	Cat#Z122882-25EA
Durapore membrane filters 0.45um HV	Millipore	Cat#HLVP02500
D-glucose (U-$^{13}C_6$, 99%)	Cambridge Isotope Laboratories	Cat#CLM 1396 PK
L-glutamine (13C5, 99%)	Cambridge Isotope Laboratories	Cat#CLM-1822-H-0.25
Sodium acetate (1,2-$^{13}C_2$, 99%)	Cambridge Isotope Laboratories	Cat#CLM-440-1
Dimethyl 2-oxoglutarate	Sigma-Aldrich	Cat#349631-5G
Critical Commercial Assays		
RNAProtect	Qiagen	Cat#76526
RNeasy Mini kit	Qiagen	Cat#74106
Baseline-ZERO DNase	Epicentre	Cat#DB0715K
Ribo-Zero rRNA Removal Kit (Gram-Negative Bacteria)	Illumina	Cat#MRZGN126
ScriptSeq RNA-Seq Library Preparation Kit	Illumina	Cat#SSV21124
Deposited Data		
Raw RNAseq data	This study	ArrayExpress: E-MTAB-6412
B. thetaiotaomicron VPI-5482 reference genome (NC_004663)	PMID_12663928	https://www.ncbi.nlm.nih.gov/nuccore/NC_004663
Experimental Models: Organisms/Strains		
Mouse: Swiss Webster	Taconic	Tac: SW-F. SW-M. RRID:IMSR_TAC:sw
Oligonucleotides		
Bt0700A-F forward primer for the flanking region A: TATCGAATTCCTGCAGCCGATTGTGACCAGGCTTTA	This study	N/A
Bt0700A-R reverse primer for the flanking region A: CGTCGAATTAACAAGATTGAATATGTAAGCACTCTATGCTAACAACAAATC	This study	N/A
Bt0700B-F forward primer for the flanking region B: GATTTGTTGTTAGCATAGAGTGCTTACATATTCAATCTTGTTAATTCGACG	This study	N/A
Bt0700B-R reverse primer for the flanking region B: GGCGGCCGCTCTAGAGTTCGCGATGTTCGGTAGAG	This study	N/A
BT3998A-F forward primer for the flanking region A: TATCGAATTCCTGCAGATTCGGGAATGGACTTCTCC	This study	N/A
BT3998A-R reverse primer for the flanking region A: CGAATGAAAGGATAACGAATATGTAATTTATCGTCCGTCCAGTTC	This study	N/A
BT3998B-F forward primer for the flanking region B: GAACTGGACGGACGATAAATTACATATTCGTTATCCTTTCATTCG	This study	N/A
BT3998B-R reverse primer for the flanking region B: GGCGGCCGCTCTAGACGCCCGTTACTTGAAAGAGA	This study	N/A
Uni-R: CACAATATGAGCAACAAGGAATCC	PMID_18996345	N/A
BC21-F: ATGTTCGATCATCAGTTCAGTAGC	P. Degnan	N/A
BC14-F: GGCACGCCATTCTTCATCTAACTG	PMID_18996345	N/A
BC22-F: ATCGTACAAGTTATACACCGTTGC	P. Degnan	N/A
Recombinant DNA		
pExchange_tdk	PMID_18611383	N/A
pExchange_tdk_Δbt0700	This study	N/A
pExchange_tdk_Δbt3998	This study	N/A
pBNUBC21	P. Degnan	N/A
pBNUBC14	PMID_18996345	N/A
pBNUBC22	P. Degnan	N/A
Software and Algorithms		
DESeq2	PMID_25516281	
EDGE-Pro	PMID_23531787	
PATRIC database (BLAST analysis)	PMID_27899627	https://www.patricbrc.org/
Cytoscape v3.4.0	PMID_14597658	http://cytoscape.org
MassHunter Quantitative Analysis Software, version 6.0	Agilent	
MatLab 2013	Mathworks	

REAGENT or RESOURCE	SOURCE	IDENTIFIER
K-Shortest Path - Yen's algorithm	Meral Shirazipour, 2011	http://www.mathworks.com/matlabcentral/fileexchange/32513-k-shortest-path-yen-s-algorithm

CONTACT FOR REAGENT AND RESOURCE SHARING

Requests for further information and resources may be directed to and will be fulfilled by Lead Contact Andrew Goodman (andrew. goodman@yale.edu).

EXPERIMENTAL MODEL AND SUBJECT DETAILS

Microbial Strains and Growth Conditions—*Bacteroides thetaiotaomicron* VPI-5482 *tdk* (Koropatkin et al., 2008) was cultured anaerobically at 37°C in liquid TYG medium (Holdeman et al., 1977), glucose minimal medium [0.5% glucose, 100 mM KH_2PO_4 (pH 7.2), 15 mM NaCl, 8.5 mM $(NH_4)_2SO_4$, 0.5 g L^{-1} cysteine, 0.2 mM histidine, 1.9 μM hematin, 100 mM $MgCl_2$, 1.4 mM $FeSO_4$, 50 mM $CaCl_2$, 1 mg mL^{-1} vitamin K_3, and 5 ng mL^{-1} vitamin B_{12}] (Martens et al., 2008), amino acid free glucose minimal medium [in which cysteine is replaced by 4 mM dithiothreitol and 4 mM Na_2S, histidine removed and hematin replaced by Hemin-HCl] or on brain heart infusion (BHI; Becton Dickinson) agar supplemented with 10% horse blood (Quad Five). An anaerobic chamber (Coy Laboratory Products) containing 20% CO_2, 10% H_2, and 70% N_2 was used for all anaerobic microbiology procedures. *Escherichia coli* S17-1 λ pir was cultured aerobically in LB medium at 37°C. Antibiotics were added, when appropriate, at the following final concentrations: ampicillin 100 μg mL^{-1}, gentamicin 200 μg mL^{-1}, erythromycin 25 μg mL^{-1}, and tetracycline 2 μg mL^{-1}.

Gnotobiotic Animal Experiments—All experiments using mice were performed using protocols approved by the Yale University Institutional Animal Care and Use Committee. Germ-free Swiss Webster mice were maintained in plastic gnotobiotic isolators with a 12 hour light/dark cycle. Individually caged animals (n = 5 per group, littermates of mixed sex were randomly assigned to experimental groups) were fed a standard, autoclaved mouse chow (5K67 LabDiet, Purina) *ad libitum*. In all experiments, mice were 12–21 weeks of age at the time of gavage; within an experiment, mice were age-matched within 2 weeks.

METHOD DETAILS

Genetic Techniques—DNA purification, PCR, and restriction cloning were performed using standard methods. Primer sequences are provided in Key Resources Table. In-frame, unmarked, nonpolar deletions were generated using a counterselectable allelic exchange procedure (Koropatkin et al., 2008) and confirmed by sequencing. Oligonucleotide barcodes in pNBU2 vectors were introduced into the genome in single copy as described (Martens et al., 2008).

***In Vitro* Growth Assays—**Individual colonies from BHI-blood agar plates were cultured in amino acid-free glucose minimal medium with and without supplementation with 20 amino acids at 0.5 mM each for 16 hours, and back-diluted to OD_{600}=0.0005. Bacterial growth rates were calculated from OD_{600} measurements collected over 30 hours on a Biotek

Eon Microplate Spectrophotometer and significant differences were determined by Tukey's HSD test.

Survival Assays during Carbon Starvation—Individual colonies from BHI-blood agar plates were cultured in glucose minimal medium in triplicate for 16 hours, and back-diluted to OD_{600}=0.0001. After reaching OD_{600}=0.4, cultures were pelleted and washed once in pre-warmed minimal medium without glucose, resuspended in pre-warmed minimal medium without glucose, and incubated for up to 100 hours at 37°C under anaerobic conditions. Cell viability was monitored by CFU (colony forming unit) counting on BHI-blood agar plates. Significant differences were determined by repeated measures ANOVA and post hoc Tukey's HSD test.

Mouse Colonization Experiments—For the competition experiments, barcoded bacterial strains were cultured individually for 16 hours in glucose minimal medium, combined (1:10:10 wildtype:*bt0700*::ppGpp^0 strains) and 10^8 CFUs were administered to each animal by oral gavage. For the community co-colonization experiments, animals were colonized with 10^8 CFU of each species in the 6- or 7-member human commensal communities described in Table S3 together with 10^8 CFUs of combined (1:10:10 wildtype:*bt0700*::ppGpp^0) barcoded *B. thetaiotaomicron* strains. Fecal samples were collected over a time course of 15–24 days and frozen immediately at −80°C. For monocolonization studies, animals were colonized with 10^8 CFUs of a single bacterial culture, fecal samples were collected over 6 days and frozen immediately at −80°C. Total gDNA was recovered from the gavage material and fecal samples, and strain abundances were determined using qPCR targeting strain-specific barcodes or genes as described (Cullen et al., 2015). Significant differences were determined by repeated measures ANOVA and post hoc Tukey's HSD test. In the sequential colonization experiments, significant differences were determined by t-test with FDR adjustment for multiple hypotheses testing with Benjamini-Hochberg procedure. For the RNAseq measurements, monocolonized mice were euthanized 6 days after gavage, cecal material was collected, immediately frozen in liquid nitrogen and stored at −80°C until further processing.

RNAseq Sample Preparation and Analysis

In Vitro Sample Preparation: For *in vitro* RNAseq measurements, individual colonies from BHI-blood agar plates where cultured in glucose minimal medium in triplicate for 16 hours, and back-diluted to OD_{600}=0.0001. After reaching OD_{600}=0.4, 5 mL of culture were combined with 10 mL RNAProtect (Qiagen), vortexed for 5 seconds, incubated for 2 minutes, pelleted by spinning for 2 minutes at 7,000 G and the pellet was stored at −80°C until further processing. For starvation profiling, 5 mL of the same culture were pelleted anaerobically by spinning at 7,000 G for 30 seconds, resuspended in 20 mL of pre-warmed minimal medium without glucose, pelleted and resuspended in 10 mL of the same medium, and incubated at 37°C under anaerobic conditions. After 1 hour, 5 mL of culture were collected, combined with RNAProtect and processed as described above. RNA was purified by resuspending cell pellets in 200 µl lysis buffer (10mM tris, 1mM ETDA, 5 mg mL^{-1} lysozyme (Sigma), 12.5 µg mL^{-1} proteinase K (pH=8.0) followed by incubation at room temperature (RT) for 10 minutes. RNA was cleaned using an RNeasy Mini kit (Qiagen) with

on column DNase I treatment, followed by treatment with Baseline-ZERO DNase (Epicentre), and a second cleaning by RNeasy Mini.

In Vivo Sample Preparation: For *in vivo* RNAseq measurements, aliquots of ~100 mg of frozen cecal samples were thawed in 1 mL of RNAProtect, resuspended, incubated at RT for 2 minutes, and pelleted by centrifugation for 1 minute at 15,000 G at 4°C. RNA was then purified as described (Rey et al., 2010). Briefly, pellets were resuspended in a solution containing 250 μL of acid-washed glass beads (Sigma-Aldrich), 500 μL of extraction buffer A (200 mM NaCl, 20 mM EDTA), 210 μL of 20% SDS, and 500 μL of phenol:chloroform:isoamyl alcohol (125:24:1, pH 4.5; Ambion), and lysed in a bead beater (BioSpec Products). Cellular debris was removed by centrifugation (8,000 G, 3 min). The extraction was repeated, and the nucleic acids were precipitated with isopropanol and sodium acetate (pH 5.5). The crude extracts were cleaned by RNeasy Mini (Qiagen) with on column DNase I treatment, treated with Baseline-ZERO DNase (Epicentre), and cleaned again by RNeasy Mini. Four RNA extracts per mouse were pooled. For both *in vitro* and *in vivo* samples, RNA quality was assayed on 2100 Bioanalyzer (Agilent), and only samples with RIN score above 8 were used for RNAseq measurements.

Preparation and Sequencing of mRNA Libraries: rRNA was depleted using the Ribo-zero rRNA removal kit for gram-negative bacteria (Illumina). RNAseq libraries were prepared using ScriptSeq v2 kit (Illumina) with multiplexing, as recommended by the manufacturer. RNAseq measurements were performed at the Yale Center for Genome Analysis using a HiSeq2000 sequencer and 1x75 bp sequencing to generate ~10–30 million reads per sample.

(p)ppGpp Labeling—Cells were cultured anaerobically in low phosphate glucose minimal medium [0.5% glucose, 1.5 mM KH_2PO_4 (pH 7.2), 2X MOPS (pH 7.2) 15 mM NaCl, 8.5 mM $(NH_4)_2SO_4$, 4 mM L-Cysteine, 5 ng mL^{-1} haemin chloride, 100 mM $MgCl_2$, 1.4 mM $FeSO_4$, 50 mM $CaCl_2$, 1 mg mL^{-1} vitamin K_3, and 5 ng mL^{-1} vitamin B_{12}]. After reaching OD_{600}=0.25, 960 μL of culture were removed from the anaerobic chamber for the remainder of the experiment in a microcentrifuge tube, supplemented with 40 μL of 2550 μCi mL^{-1} $KH_2{}^{32}PO_4$ (PerkinElmer, Waltham, MA, USA), and incubated at 37°C for 2 hours. At this point, a 160 μl aliquot was removed and nucleotides were extracted. The remaining culture was pelleted, resuspended in pre-warmed low phosphate minimal medium without glucose, incubated for 1 hour at 37°C, and nucleotides were extracted from 160 μl of culture. Nucleotides were extracted by the addition of 40 μL 10 M ice-cold formic acid plus glass beads, 15 seconds vortexing, incubation on ice for 20 minutes, 5 seconds vortexing, and incubation on dry ice for 20 minutes. These samples were thawed, vortexed for 5 seconds, and centrifuged for 1 minute at 20,000 G to remove cell debris. To analyze labeled nucleotides by thin-layer chromatography, 3 μL of extract was spotted on PEI-cellulose TLC sheets (Sigma) and developed in 1.5 M KH_2PO_4 (pH 3.9). TLC plates were imaged with a Typhoon Phosphoscanner and analyzed with QuantityOne software.

Metabolomics Experiments

Sample Preparation: Intracellular metabolites were extracted in the anaerobic chamber at 37°C as previously described (Link et al., 2013). In brief, biomass equivalents corresponding to 1 mL bacterial culture at OD_{600} 2.0 were filtered through 0.45 μm filter membranes (HVLP, Millipore, Billerica, MA, USA) prewarmed with medium, and filtered bacteria were washed with 2 mL prewarmed, fresh medium. Filters were rapidly transferred to 2 mL of extraction solution (acetonitrile:methanol:water (2:2:1), 100 mM formic acid) and 200 μL of ^{13}C-labeled internal standard were added. Extraction solutions were kept at −20°C for 1 hour, dried under vacuum at 22°C, resuspended in 60 μL H_2O, centrifuged for 1 minute at 21,000 G, and supernatant was removed for further analysis.

Targeted Metabolomics: Targeted metabolite quantification was carried out using an Agilent 1290 UHPLC system coupled to an Agilent 6490A QqQ mass spectrometer. Chromatographic separation was performed on a Luna NH2 column (Phenomenex, 50 x 3 mm, 3 μm particle size) using mobile phase A: 20 mM ammonium acetate buffer (pH 9.45) with 5% acetonitrile and B: acetonitrile (Bajad et al., 2006). 7.5 μL of sample were injected at 15% B followed by a linear gradient to 50% B over 3 min and to 98% over 17 min with subsequent isocratic conditions at 98% for 12 min. The flow was kept constant at 0.6 mL min^{-1} and the column was re-equilibrated at starting conditions for 8 min. The QqQ was operated in negative ionization mode using dynamic MRM scan settings with the following source parameters: VCap: 3500 V, nozzle voltage: 2000 V, gas temperature: 275°C; drying gas 12 L min^{-1}; nebulizer: 35 psig; sheath gas temperature 275°C; sheath gas flow 12 L min^{-1}. MRM parameters were optimized for each compound (Table S5) separately following the manufacturer's recommendation using direct injection of chemical standards. ^{13}C-labeled internal standard solution was prepared from *E. coli* MG1655 cultured in M9 minimal medium [22 mM KH_2PO_4, 22 mM Na_2HPO_4, 85 mM NaCl, 0.1% NH_4Cl, 0.2 mM $MgSO_4$, 0.1 mM $CaCl_2$, 0.4% [U-^{13}C]-glucose (Cambridge Isotope Laboratories)]. After reaching OD_{600}=0.6, cells were filtered and extracted as described above at a ratio of 20 OD_{600} to 2 mL of extraction solution. The MassHunter Quantitative Analysis Software (Agilent, version 6.0) was used for peak integration and quantification was based on calibration curves using chemical standards and the signal intensity of the internal standard spiked into each sample.

Untargeted Metabolomics: Untargeted metabolomics was carried out using an Agilent 1290 UHPLC system coupled to an Agilent 6550 qTOF mass spectrometer. Chromatographic separation was performed on a ZIC-pHILIC column (Merck, 150 mm × 2.1 mm, 5 μm particle size) using mobile phase A: 10 mM ammonium carbonate buffer (pH 9.3) and B: acetonitrile. 3 μL of sample were injected at 80% B and 0.1 mL min^{-1} flow followed by a linear gradient to 50% B over 20 min and 0.1 mL min^{-1} flow (Chaleckis et al., 2014). The column was re-equilibrated at starting conditions for 8 min. The qTOF was operated in positive (50 – 1000 m/z) and negative (50 – 1050 m/z) scanning mode and source parameters optimized following the manufacturer's recommendations: VCap: 3500 V, nozzle voltage: 2000 V, gas temp: 225°C; drying gas 13 L min^{-1}; nebulizer: 20 psig; sheath gas temp 225°C; sheath gas flow 12 L min^{-1}. Online mass calibration was performed using a second ionization source and a constant flow (5 μL min^{-1}) of reference solution

(positive mode: 121.0509 and 922.0098 m/z and negative mode: 112.9856 and 1033.9881 m/z).

^{13}C Labeling Experiments

Growth Experiments: To monitor carbon flux during growth in glucose, cells were cultured in minimal medium with 0.3% unlabeled glucose to OD_{600}=0.4 in an anaerobic chamber heated to 37°C and transferred to a prewarmed filter membrane as described for metabolomics extractions. Medium switch was performed under continual flow of minimal medium with 0.3% of 100% [U-^{13}C]-glucose (Cambridge Isotope Laboratories CLM-1396-PK) for up to 5 minutes, and metabolites were extracted after 10, 20, 40, 80, 160 and 320 seconds as described above (without the spike-in of the ^{13}C labeled internal standard). The acetate growth shift experiment was conducted following the same procedure, with the cells grown in minimal medium containing 0.3% unlabeled glucose and 0.1% unlabeled acetate and switched to medium containing 0.3% unlabeled glucose and 0.1% of 100% [U-^{13}C]-acetate (Cambridge Isotope Laboratories).

Starvation Experiments: To monitor carbon flux from acetate during starvation, cells were cultured in minimal medium with 0.3% unlabeled glucose and 0.1% of 100% [U-^{13}C]-acetate to OD_{600}=0.4, pelleted, washed twice in minimal medium without glucose containing 0.1% of 100% [U-^{13}C]-acetate, and incubated in the same medium for up to 20 hours. Metabolites were extracted at 1, 5, 15 and 19 hours as described for metabolomics measurements (without the ^{13}C internal standard). To monitor carbon flux from glutamine during starvation, cells were cultured in minimal medium lacking $(NH_4)_2SO_4$ in the presence of 0.3% unlabeled glucose and 1mM unlabeled glutamine as the sole nitrogen source, grown to OD_{600}=0.4, pelleted, and washed twice in the same minimal medium except unlabeled glucose and glutamine were omitted and 0.25 mM 100% [U-^{13}C]-glutamine (Cambridge isotope Laboratories) was included. Cultures were incubated in this medium for up to 20 hours. Metabolites were extracted at 1, 3, 5, 9, and 20 hours as described for metabolomics measurements (without the ^{13}C internal standard). Metabolite isotopomers were quantified by LC-MS/MS as described for targeted metabolomics measurements using separate transitions for each possible mass isomer. Isotope fractions were calculated by normalizing each isotopomer intensity by the sum of intensities of all isotopomers detected for the same metabolite.

Alpha-Ketoglutarate and Glutamine Supplementation Experiments—To test the effect of AKG supplementation on growing cells, *B. thetaiotaomicron* wildtype and ppGpp^0 strains were cultured in glucose minimal medium to OD_{600}=0.1 and supplemented with 1 mM dimethyl-AKG from a 1 M DMSO stock (Sigma). Growth was monitored for 8 hours by OD_{600} measurements with a microplate spectrophotometer (Biotek Eon). To test the effect of AKG and glutamine on *B. thetaiotaomicron* viability during starvation, wildtype and ppGpp^0 strains were grown in glucose minimal medium to OD_{600}=0.3. Each culture was divided into three subcultures and supplemented with 1 mM of either dimethyl-AKG, DMSO as a dimethyl-AKG vehicle control, or glutamine. After 30 minutes, cells were pelleted and washed twice in minimal medium lacking glucose and supplemented with 1 mM dimethyl-AKG, DMSO, or glutamine to match the 30 minute incubation of that culture.

Cultures were resuspended in the same medium and incubated for 40 hours. Cell viability was monitored by CFU counting on BHI-blood plates. Metabolites were extracted by filtration as described for metabolomics experiments from ppGpp^0 samples before and 0, 1, 3, 5, 10 and 20 hours after the wash step and measured with liquid chromatography-coupled mass spectrometry (LC-qTOF).

QUANTIFICATION AND STATISTICAL ANALYSIS

BLAST Alignment of (p)ppGpp Synthases—Nucleotide sequence alignment to (p)ppGpp synthetase/hydrolase RelSeq gene from Gammaproteobacterium *Streptococcus equisimilis* (Table S1) was performed using BLAST service of the PATRIC database (Wattam et al., 2017) for reference genomes of *B. thetaiotaomicron*, *B. ovatus*, *B. eggerthii*, *B. uniformis*, and *B. vulgatus.*

Analysis of Starvation and Competition Assays—Growth, starvation and mouse colonization datasets were analyzed in MatLab 2013 (Mathworks). Growth rates of WT, *bt0700* and ppGpp^0 strains were compared with Tukey's HSD test (multcompare function with 'hsd' option). Time-course starvation and mouse colonization data were analyzed with repeated measures ANOVA (ranova function). Statistical significance of pairwise comparisons between genotypes within each timepoint was assessed with Tukey's HSD test. P-values were adjusted for multiple hypothesis testing with Benjamini-Hochberg procedure (mafdr function with 'bhfdr' option). P-values, FDR and n values are indicated in the associated figure legends for each figure and in Tables S3, S4, S5, S6, and S7.

RNAseq Data Mapping—RNAseq sequences were aligned to the *B. thetaiotaomicron* VPI-5482 reference genome (NC_004663) (Xu et al., 2003) using EDGE-Pro (Magoc et al., 2013) and reads were normalized using DESeq2 (Love et al., 2014).

Metabolomic Data Filtering and Annotation—Ions were annotated to metabolites based on exact mass considering [M-H$^+$] and [M+H$^+$] ions using the metabolite reference list compiled from the Kyoto Encyclopedia of Genes and Genomes (KEGG) metabolite repository bth (*B. thetaiotaomicron*) (Ogata et al., 1999). Ions were assigned to metabolites allowing a mass tolerance of 1 mDa and an intensity cutoff of 5,000 counts. Reference retention times of pure chemical standards measured with the same settings were used for annotation, when available. Raw intensity values were quantile-normalized with quantnorm function in MatLab 2013a (MathWorks). For each metabolite, only the annotation with the top score was retained. The concentration of intercellular ppGpp was determined by LC-qTOF using the procedure described above and a standard curve established using a pure ppGpp standard (TriLink) with a linear detection range of 1 nM – 1 μM.

RNAseq and Metabolomics Data Analysis—Metabolomics and RNAseq data were imported into MatLab 2013a (MathWorks) for quantitative and statistical analysis. Principal component analysis was performed on $\log_2$-transformed RNAseq data normalized by mean expression of each gene with the pca function in MatLab. For differential analysis, pairwise comparisons were performed with $\log_2$-transformed normalized RNAseq reads between genotypes in each condition, and between conditions within each genotype using Welch test

(t-test with unequal variances) with two to four biological replicates per condition. Log_2-transformed normalized metabolite intensities were compared between genotypes in each condition, and between conditions within each genotype using Welch test with three biological replicates per condition. P-values were corrected for multiple hypotheses testing by calculating the false-discovery rate (FDR) with the Benjamini-Hochberg procedure (mafdr function in MatLab).

Pathway Enrichment Analysis—For pathway enrichment analysis, pathway descriptions were downloaded from the KEGG database, and the gene set enrichment analysis (GSEA) method (Subramanian et al., 2005) was applied as described (Zimmermann et al., 2017). Significantly changing transcripts and metabolites ($|\log_2(\text{fold change})| \geq 1$, FDR ≤ 0.05 for transcripts and $|\log_2(\text{fold change})| \geq \log_2(1.5)$, FDR ≤ 0.05 for metabolites) were ranked either by fold change or by FDR, and enrichment p-values were calculated with the Fisher exact test for each subset of size varying from 1 to the total changing set size. For each pathway, the smallest p-value of all the subsets was retained, and p-values were adjusted for multiple hypotheses testing by calculating FDR with the Benjamini-Hochberg procedure. In AKG supplementation experiments, pathway enrichment was performed for metabolites that follow each of the rules: 1) $|\log_2(\text{fold change in starvation versus growth})| \geq \log_2(1.5)$ in at least 3 time points either with or without AKG supplementation; 2) $|\log_2(\text{fold change in starvation with AKG compared to no AKG})| \geq \log_2(1.5)$ in at least 3 time points; 3) area between the metabolite profile curves with and without AKG supplementation ≥ 50% of the total area. Metabolites were sorted according to the area under the curve difference between conditions in descending order.

Reaction Pair Network Analysis—For KEGG reaction pair network analysis, the KEGG reaction pair list, KEGG reaction pair – *B. thetaiotaomicron* gene association list, and KEGG compound list were downloaded from KEGG API (application programming interface) (http://rest.kegg.jp/, accessed July 2015), and only the main (substrate-product) reaction pairs were retained. These datasets were used to define the list of metabolites involved in reactions associated with each gene. A gene-gene connectivity matrix was built based on the metabolites associated with the genes (if two genes are associated with reactions sharing a metabolite, they are connected through this metabolite). K-shortest path script based on Yen's algorithm (Yen, 1971) (implementation by Meral Shirazipour (2011) K-Shortest Path - Yen's algorithm http://ninwww.mathworks.com/matlabcentral/fileexchange/32513-k-shortest-path-yen-s-algorithm, accessed July 2015) was used to calculate the shortest paths between two genes based on the connectivity matrix. All paths of length four and more which connect $ppGpp^0$-specific changing genes ($|\log_2(\text{fold change})| \geq 1$, FDR ≤ 0.05 in $ppGpp^0$ compared to wildtype and *bt0700*, but not between wildtype and *bt0700 in vivo*, one unchanged reaction allowed) were represented as a table and visualized in Cytoscape software (Cytoscape 3.4.0) (Shannon et al., 2003). Subnetworks were manually grouped and assigned to KEGG pathways for better visualization.

DATA AVAILABILITY

The raw RNAseq data have been deposited in the EMBL-EBI European Nucleotide Archive under accession no. E-MTAB-6412. The metabolomics data are provided in Tables S5, S6, and S7.

Supplementary Material

Refer to Web version on PubMed Central for supplementary material.

Acknowledgments

We thank E. Groisman, H. Kornberg, and members of the Goodman lab for helpful discussions. This work was supported by NIH grants GM105456, GM103574, GM118159, AI124275, the Burroughs Wellcome Fund, and the HHMI Faculty Scholars Program to A.L.G. M.Z.-K. and M.Z. received Early Postdoc Mobility Fellowships from the Swiss National Science Foundation (P2EZP3_178482 and P2EZP3_162256, respectively) and M.Z. received a Long-Term Fellowship (ALTF 670-2016) from the European Molecular Biology Organization.

References

Amador-Noguez D, Feng X-J, Fan J, Roquet N, Rabitz H, Rabinowitz JD. Systems-level metabolic flux profiling elucidates a complete, bifurcated tricarboxylic acid cycle in *Clostridium acetobutylicum*. J Bacteriol. 2010; 192:4452–4461. [PubMed: 20622067]

Atkinson GC, Tenson T, Hauryliuk V. The RelA/SpoT homolog (RSH) superfamily: distribution and functional evolution of ppGpp synthetases and hydrolases across the tree of life. PLoS One. 2011; 6:e23479. [PubMed: 21858139]

Bajad SU, Lu W, Kimball EH, Yuan J, Peterson C, Rabinowitz JD. Separation and quantitation of water soluble cellular metabolites by hydrophilic interaction chromatography-tandem mass spectrometry. J Chromatogr A. 2006; 1125:76–88. [PubMed: 16759663]

Baughn AD, Malamy MH. A mitochondrial-like aconitase in the bacterium *Bacteroides fragilis*: implications for the evolution of the mitochondrial Krebs cycle. Proc Natl Acad Sci USA. 2002; 99:4662–4667. [PubMed: 11880608]

Bojanova DP, Bordenstein SR. Fecal transplants: what is being transferred? PLoS Biol. 2016; 14:e1002503. [PubMed: 27404502]

Boutte CC, Crosson S. The complex logic of stringent response regulation in *Caulobacter crescentus*: starvation signalling in an oligotrophic environment. Mol Microbiol. 2011; 80:695–714. [PubMed: 21338423]

Boutte CC, Crosson S. Bacterial lifestyle shapes stringent response activation. Trends Microbiol. 2013; 21:174–180. [PubMed: 23419217]

Braeken K, Moris M, Daniels R, Vanderleyden J, Michiels J. New horizons for (p)ppGpp in bacterial and plant physiology. Trends Microbiol. 2006; 14:45–54. [PubMed: 16343907]

Cashel M, Gentry DR, Hernandez VJ, Vinella D. The stringent response*Escherichia coli* and Salmonella. In: Neidhardt FC, Curtiss R, , IIIIngraham JL, Lin ECC, Low KB, Magasanik B, Reznikoff W, Riley M, Schaechter M, Umbarger AE, editorsCellular and Molecular Biology. ASM Press; 1996. 913–931.

Chaleckis R, Ebe M, Pluskal T, Murakami I, Kondoh H, Yanagida M. Unexpected similarities between the *Schizosaccharomyces* and human blood metabolomes, and novel human metabolites. Mol Biosyst. 2014; 10:2538–2551. [PubMed: 25010571]

Chen X, Alonso AP, Allen DK, Reed JL, Shachar-Hill Y. Synergy between ^{13}C-metabolic flux analysis and flux balance analysis for understanding metabolic adaption to anaerobiosis in *E. coli*. Metab Eng. 2011; 13:38–48. [PubMed: 21129495]

Chin RM, Fu X, Pai MY, Vergnes L, Hwang H, Deng G, Diep S, Lomenick B, Meli VS, Monsalve GC, et al. The metabolite α-ketoglutarate extends lifespan by inhibiting ATP synthase and TOR. Nature. 2014; 510:397–401. [PubMed: 24828042]

Cullen TW, Schofield WB, Barry NA, Putnam EE, Rundell EA, Trent MS, Degnan PH, Booth CJ, Yu H, Goodman AL. Antimicrobial peptide resistance mediates resilience of prominent gut commensals during inflammation. Science. 2015; 347:170–175. [PubMed: 25574022]

Dahl JL, Kraus CN, Boshoff HIM, Doan B, Foley K, Avarbock D, Kaplan G, Mizrahi V, Rubin H, Barry CE. The role of RelMtb-mediated adaptation to stationary phase in long-term persistence of *Mycobacterium tuberculosis* in mice. Proc Natl Acad Sci USA. 2003; 100:10026–10031. [PubMed: 12897239]

Dalebroux ZD, Swanson MS. ppGpp: magic beyond RNA polymerase. Nat Rev Microbiol. 2012; 10:203–212. [PubMed: 22337166]

Dalebroux ZD, Svensson SL, Gaynor EC, Swanson MS. ppGpp conjures bacterial virulence. Microbiol Mol Biol Rev. 2010; 74:171–199. [PubMed: 20508246]

Doucette CD, Schwab DJ, Wingreen NS, Rabinowitz JD. α-Ketoglutarate coordinates carbon and nitrogen utilization via enzyme I inhibition. Nat Chem Biol. 2011; 7:894–901. [PubMed: 22002719]

Eymann C, Homuth G, Scharf C, Hecker M. *Bacillus subtilis* functional genomics: global characterization of the stringent response by proteome and transcriptome analysis. J Bacteriol. 2002; 184:2500–2520. [PubMed: 11948165]

Fischbach MA, Sonnenburg JL. Eating for two: how metabolism establishes interspecies interactions in the gut. Cell Host Microbe. 2011; 10:336–347. [PubMed: 22018234]

de la Fuente-Núñez C, Reffuveille F, Haney EF, Straus SK, Hancock REW. Broad-spectrum anti-biofilm peptide that targets a cellular stress response. PLoS Pathog. 2014; 10:e1004152. [PubMed: 24852171]

Gaca AO, Colomer-Winter C, Lemos JA. Many means to a common end: the intricacies of (p)ppGpp metabolism and its control of bacterial homeostasis. J Bacteriol. 2015; 197:1146–1156. [PubMed: 25605304]

Glass TL, Holmes WM, Hylemon PB, Stellwag EJ. Synthesis of guanosine tetra- and pentaphosphates by the obligately anaerobic bacterium *Bacteroides thetaiotaomicron* in response to molecular oxygen. J Bacteriol. 1979; 137:956–962. [PubMed: 422517]

Goodman AL, McNulty NP, Zhao Y, Leip D, Mitra RD, Lozupone CA, Knight R, Gordon JI. Identifying genetic determinants needed to establish a human gut symbiont in its habitat. Cell Host Microbe. 2009; 6:279–289. [PubMed: 19748469]

Haralalka S, Nandi S, Bhadra RK. Mutation in the relA gene of *Vibrio cholerae* affects in vitro and in vivo expression of virulence factors. J Bacteriol. 2003; 185:4672–4682. [PubMed: 12896985]

Haseltine WA, Block R. Synthesis of guanosine tetra- and pentaphosphate requires the presence of a codon-specific, uncharged transfer ribonucleic acid in the acceptor site of ribosomes. Proc Natl Acad Sci USA. 1973; 70:1564–1568. [PubMed: 4576025]

Hauryliuk V, Atkinson GC, Murakami KS, Tenson T, Gerdes K. Recent functional insights into the role of (p)ppGpp in bacterial physiology. Nat Rev Microbiol. 2015; 13:298–309. [PubMed: 25853779]

Hogg T, Mechold U, Malke H, Cashel M, Hilgenfeld R. Conformational antagonism between opposing active sites in a bifunctional RelA/SpoT homolog modulates (p)ppGpp metabolism during the stringent response. Cell. 2004; 117:57–68. [PubMed: 15066282]

Holdeman LV, Cato EP, Moore WE. Anaerobe Laboratory Manual. Virginia Polytechnic Institute and State University Anaerobe Laboratory; 1977.

Irnov I, Wang Z, Jannetty ND, Bustamante JA, Rhee KY, Jacobs-Wagner C. Crosstalk between the tricarboxylic acid cycle and peptidoglycan synthesis in *Caulobacter crescentus* through the homeostatic control of α-ketoglutarate. PLoS Genet. 2017; 13:e1006978. [PubMed: 28827812]

Jishage M, Kvint K, Shingler V, Nyström T. Regulation of sigma factor competition by the alarmone ppGpp. Genes Dev. 2002; 16:1260–1270. [PubMed: 12023304]

Kanjee U, Ogata K, Houry WA. Direct binding targets of the stringent response alarmone (p)ppGpp. Mol Microbiol. 2012; 85:1029–1043. [PubMed: 22812515]

Kazmierczak KM, Wayne KJ, Rechtsteiner A, Winkler ME. Roles of rel(Spn) in stringent response, global regulation and virulence of serotype 2 *Streptococcus pneumoniae* D39. Mol Microbiol. 2009; 72:590–611. [PubMed: 19426208]

Koropatkin NM, Martens EC, Gordon JI, Smith TJ. Starch catabolism by a prominent human gut symbiont is directed by the recognition of amylose helices. Structure. 2008; 16:1105–1115. [PubMed: 18611383]

Koropatkin NM, Cameron EA, Martens EC. How glycan metabolism shapes the human gut microbiota. Nat Rev Microbiol. 2012; 10:323–335. [PubMed: 22491358]

Krásný L, Gourse RL. An alternative strategy for bacterial ribosome synthesis: *Bacillus subtilis* rRNA transcription regulation. EMBO J. 2004; 23:4473–4483. [PubMed: 15496987]

Lee SM, Donaldson GP, Mikulski Z, Boyajian S, Ley K, Mazmanian SK. Bacterial colonization factors control specificity and stability of the gut microbiota. Nature. 2013; 501:426–429. [PubMed: 23955152]

Lemke JJ, Durfee T, Gourse RL. DksA and ppGpp directly regulate transcription of the *Escherichia coli* flagellar cascade. Mol Microbiol. 2009; 74:1368–1379. [PubMed: 19889089]

Link H, Kochanowski K, Sauer U. Systematic identification of allosteric protein-metabolite interactions that control enzyme activity in vivo. Nat Biotechnol. 2013; 31:357–361. [PubMed: 23455438]

Liu K, Bittner AN, Wang JD. Diversity in (p)ppGpp metabolism and effectors. Curr Opin Microbiol. 2015; 24:72–79. [PubMed: 25636134]

Love MI, Huber W, Anders S. Moderated estimation of fold change and dispersion for RNA-seq data with DESeq2. Genome Biol. 2014; 15:550. [PubMed: 25516281]

Magoc T, Wood D, Salzberg SL. EDGE-pro: estimated degree of gene expression in prokaryotic genomes. Evol Bioinform Online. 2013; 9:127–136. [PubMed: 23531787]

Martens EC, Chiang HC, Gordon JI. Mucosal glycan foraging enhances fitness and transmission of a saccharolytic human gut bacterial symbiont. Cell Host Microbe. 2008; 4:447–457. [PubMed: 18996345]

Maurice CF, Haiser HJ, Turnbaugh PJ. Xenobiotics shape the physiology and gene expression of the active human gut microbiome. Cell. 2013; 152:39–50. [PubMed: 23332745]

Myhrvold C, Kotula JW, Hicks WM, Conway NJ, Silver PA. A distributed cell division counter reveals growth dynamics in the gut microbiota. Nat Commun. 2015; 6:10039. [PubMed: 26615910]

Ogata H, Goto S, Sato K, Fujibuchi W, Bono H, Kanehisa M. KEGG: Kyoto encyclopedia of genes and genomes. Nucleic Acids Res. 1999; 27:29–34. [PubMed: 9847135]

Pizarro-Cerdá J, Tedin K. The bacterial signal molecule, ppGpp, regulates *Salmonella* virulence gene expression. Mol Microbiol. 2004; 52:1827–1844. [PubMed: 15186428]

Potrykus K, Cashel M. (p)ppGpp: still magical? Annu Rev Microbiol. 2008; 62:35–51. [PubMed: 18454629]

Rey FE, Faith JJ, Bain J, Muehlbauer MJ, Stevens RD, Newgard CB, Gordon JI. Dissecting the in vivo metabolic potential of two human gut acetogens. J Biol Chem. 2010; 285:22082–22090. [PubMed: 20444704]

Ross W, Vrentas CE, Sanchez-Vazquez P, Gaal T, Gourse RL. The magic spot: a ppGpp binding site on *E. coli* RNA polymerase responsible for regulation of transcription initiation. Mol Cell. 2013; 50:420–429. [PubMed: 23623682]

Sauer U, Lasko DR, Fiaux J, Hochuli M, Glaser R, Szyperski T, Wüthrich K, Bailey JE. Metabolic flux ratio analysis of genetic and environmental modulations of *Escherichia coli* central carbon metabolism. J Bacteriol. 1999; 181:6679–6688. [PubMed: 10542169]

Seyfzadeh M, Keener J, Nomura M. spoT-dependent accumulation of guanosine tetraphosphate in response to fatty acid starvation in *Escherichia coli*. Biochemistry. 1993; 90:11004–11008.

Shannon P, Markiel A, Ozier O, Baliga NS, Wang JT, Ramage D, Amin N, Schwikowski B, Ideker T. Cytoscape: a software environment for integrated models of biomolecular interaction networks. Genome Res. 2003; 13:2498–2504. [PubMed: 14597658]

Sonnenburg JL, Xu J, Leip DD, Chen CH, Westover BP, Weatherford J, Buhler JD, Gordon JI. Glycan foraging in vivo by an intestine-adapted bacterial symbiont. Science. 2005; 307:1955–1959. [PubMed: 15790854]

Subramanian A, Tamayo P, Mootha VK, Mukherjee S, Ebert BL, Gillette MA, Paulovich A, Pomeroy SL, Golub TR, Lander ES, et al. Gene set enrichment analysis: a knowledge-based approach for

interpreting genome-wide expression profiles. Proc Natl Acad Sci USA. 2005; 102:15545–15550. [PubMed: 16199517]

Traxler MF, Summers SM, Nguyen H-T, Zacharia VM, Hightower GA, Smith JT, Conway T. The global, ppGpp-mediated stringent response to amino acid starvation in *Escherichia coli*. Mol Microbiol. 2008; 68:1128–1148. [PubMed: 18430135]

Vinella D, Albrecht C, Cashel M, D'Ari R. Iron limitation induces SpoT-dependent accumulation of ppGpp in *Escherichia coli*. Mol Microbiol. 2005; 56:958–970. [PubMed: 15853883]

Wattam AR, Davis JJ, Assaf R, Boisvert S, Brettin T, Bun C, Conrad N, Dietrich EM, Disz T, Gabbard JL, et al. Improvements to PATRIC, the all-bacterial Bioinformatics Database and Analysis Resource Center. Nucleic Acids Res. 2017; 45:D535–D542. [PubMed: 27899627]

Wexselblatt E, Oppenheimer-Shaanan Y, Kaspy I, London N, Schueler-Furman O, Yavin E, Glaser G, Katzhendler J, Ben-Yehuda S. Relacin, a novel antibacterial agent targeting the stringent response. PLoS Pathog. 2012; 8:e1002925. [PubMed: 23028324]

Xiao H, Kalman M, Ikehara K, Zemel S, Glaser G, Cashel M. Residual guanosine 3′,5′-bispyrophosphate synthetic activity of relA null mutants can be eliminated by spoT null mutations. J Biol Chem. 1991; 266:5980–5990. [PubMed: 2005134]

Xu J, Bjursell MK, Himrod J, Deng S, Carmichael LK, Chiang HC, Hooper LV, Gordon JI. A genomic view of the human- *Bacteroides thetaiotaomicron* symbiosis. Science. 2003; 299:2074–2076. [PubMed: 12663928]

Yen JY. Finding the K shortest loopless paths in a network. Manage Sci. 1971; 17:712–716.

Zimmermann M, Kogadeeva M, Gengenbacher M, McEwen G, Mollenkopf HJ, Zamboni N, Kaufmann SHE, Sauer U. Integration of metabolomics and transcriptomics reveals a complex diet of *Mycobacterium tuberculosis* during early macrophage infection. mSystems. 2017; 2:e00057–17. [PubMed: 28845460]

Highlights

- Gut commensal B. thetaiotaomicron uses alarmone (p)ppGpp to shift from growth to stasis
- (p)ppGpp is required for colonization in the gut of freely fed mice
- The (p)ppGpp-dependent response is recapitulated during carbon starvation in vitro
- (p)ppGpp is required to elevate α-ketoglutarate, which prolongs starvation survival

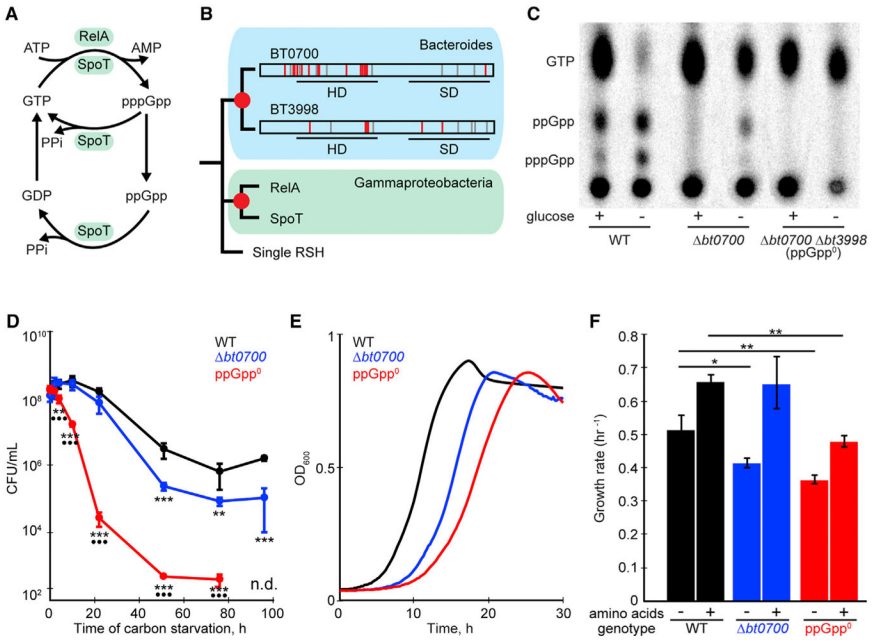

Figure 1. *Bacteroides thetaiotaomicron* Encodes Two Enzymes that Contribute to (p)ppGpp Production upon Carbon Starvation

(A) Reactions catalyzed by RelA/SpoT Homologue (RSH) proteins.

(B) Phylogenetic analysis of RSH proteins reveals independent duplication events within the Bacteroides and Gammaproteobacteria lineages. Amino acid substitutions at residues required for hydrolase or synthetase activity in homologous proteins (Hogg et al., 2004) are indicated in red (non-similar) and gray (similar). Red circles indicate predicted gene duplication events. SD, synthetase domain; HD, hydrolase domain.

(C) Thin-layer chromatography of ^{32}P-labeled nucleotide extracts from *B. thetaiotaomicron* cells before (+) and 2 hr after (−) a shift from glucose replete to glucose deplete medium.

(D) Survival of wild-type (WT), *bt0700,* and ppGpp^0 strains during prolonged carbon starvation.

(E) Growth of WT, *bt0700,* and ppGpp^0 strains in defined minimal medium without amino acids.

(F) Growth rates of WT, *bt0700,* and ppGpp^0 strains in defined minimal medium with and without amino acids.

Error bars represent SD of three biological replicates. Significant differences between WT and mutant strains are indicated with asterisks, between ppGpp^0 and *bt0700* strains with dots (*p < 0.05; **p < 0.01; ***p < 0.001, Tukey's HSD test and FDR adjustment with Benjamini-Hochberg procedure). See also Figure S1, Table S3.

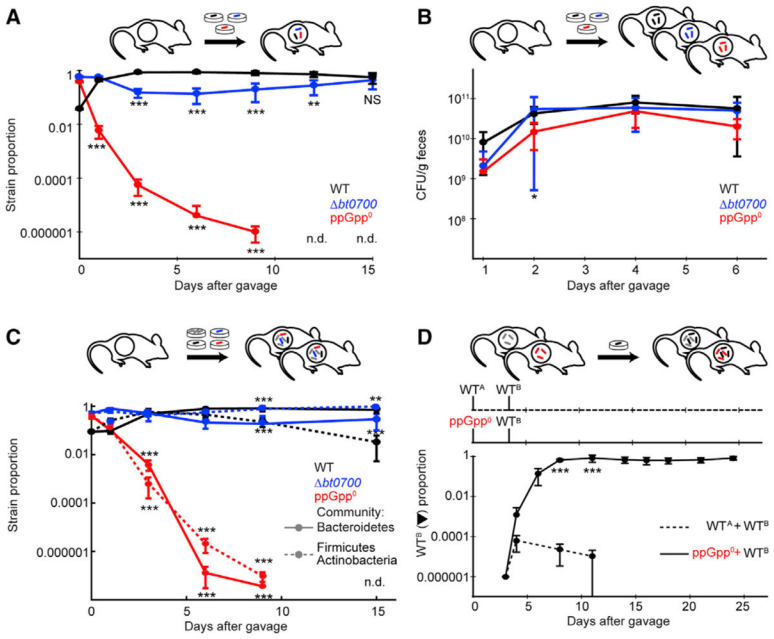

Figure 2. *B. thetaiotaomicron* Requires (p)ppGpp for Establishment and Maintenance of Mouse Gut Colonization

(A and B) Relative abundance of WT, *bt0700,* and ppGpp^0 strains in feces of gnotobiotic mice colonized with these isogenic strains together (A) or separately (B).

(C) Population dynamics of WT, *bt0700,* and ppGpp^0 strains in gnotobiotic mice carrying defined, multi-species human gut communities representing Bacteroidetes, Firmicutes, and Actinobacteria phyla.

(D) Population dynamics of a barcoded WT *B. thetaiotaomicron* strain (WT^B) in gnotobiotic mice previously colonized with either WT *B. thetaiotaomicron* (WT^A) or the ppGpp^0 strain.

Error bars represent SD of five biological replicates. Significant differences between WT and mutant strains during co-colonization are indicated with asterisks (*p < 0.05; **p < 0.01; ***p < 0.001, Tukey's HSD test (A–C) or t test (D) and FDR adjustment with Benjamini-Hochberg procedure).

See also Figure S2, Table S3.

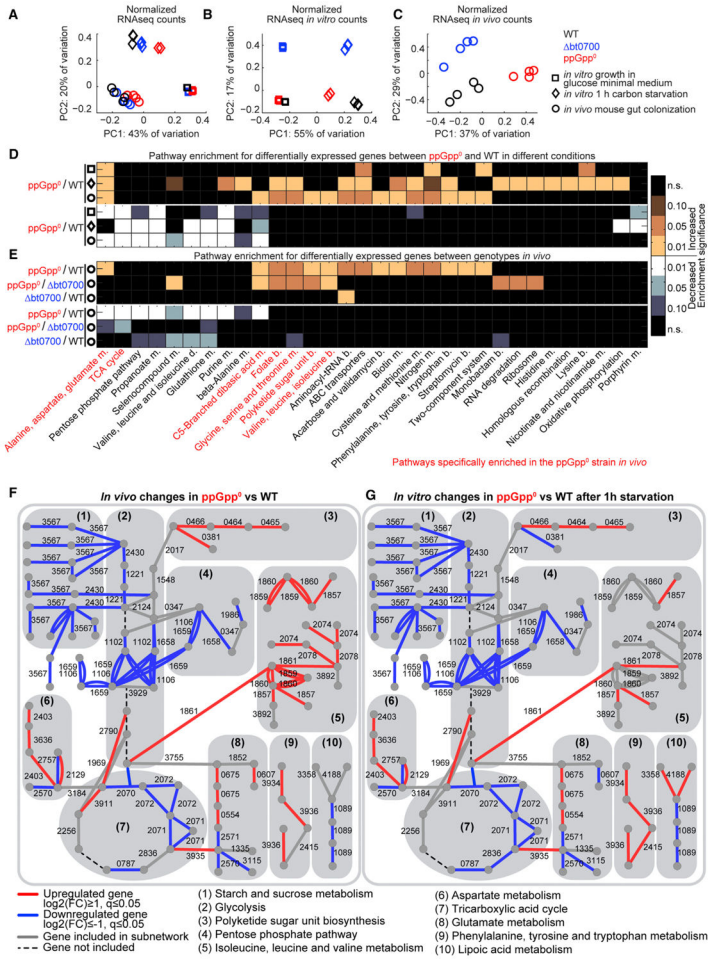

Figure 3. *B. thetaiotaomicron* Uses (p)ppGpp as a Global Transcriptional Regulator during *In Vitro* Starvation and *In Vivo* Colonization

(A) PCA of normalized RNA-seq data of WT, *bt0700,* and ppGpp^0 strains measured during exponential growth conditions *in vitro*, after 1 hr carbon starvation *in vitro,* and during growth *in vivo* in the cecum of monoassociated gnotobiotic mice.

(B and C) PCA plots of RNA-seq data from *in vitro* (B) and *in vivo* (C) conditions analyzed separately.

(D and E) KEGG pathway enrichment analysis of significantly changing genes between ppGpp^0 and WT strains across conditions (D); and between genotypes *in vivo* (E). Pathways are displayed if the enrichment p value (FDR adjusted with Benjamini-Hochberg procedure) is < 0.01 in at least one condition; black, n.s. (not significant). Pathways changing in the ppGpp^0 strain compared with WT and *bt0700 in vivo* are marked in red. m., metabolism; b., biosynthesis; d., degradation.

(F and G) Metabolic subnetworks of genes expressed at significantly different levels between ppGpp^0 and both the *bt0700* and WT genotypes, but not between *bt0700* and WT genotypes, during gut colonization. Subnetwork edges are colored according to gene fold changes between ppGpp^0 and WT *in vivo* (F) or *in vitro* after 1-hr carbon starvation (G). Edge numbering corresponds to Ref-seq locus tags.

See also Figure S3, Table S4.

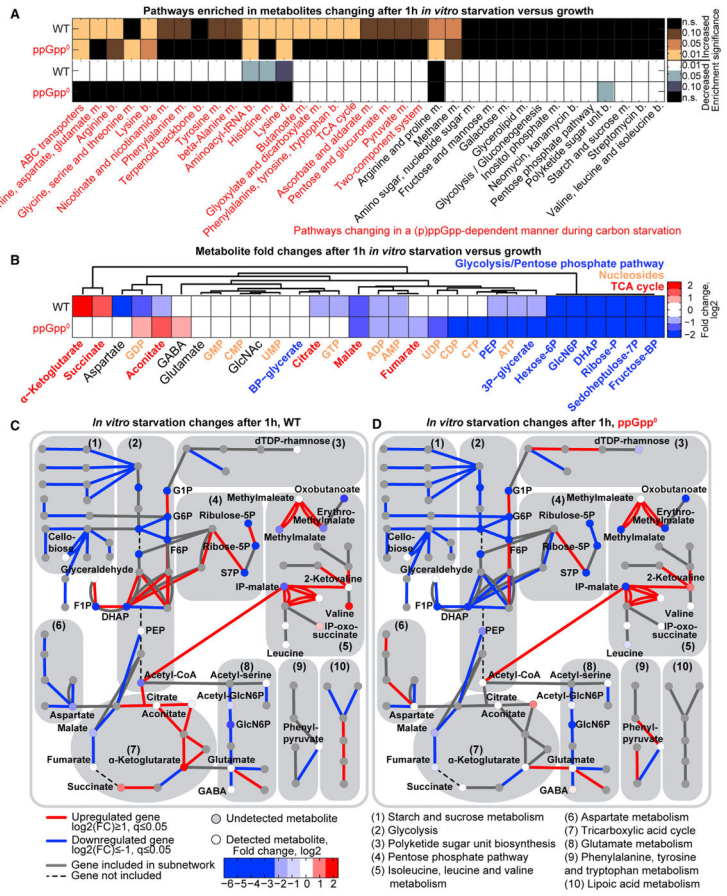

Figure 4. *B. thetaiotaomicron* Triggers Significant, (p)ppGpp-Dependent Changes in TCA Cycle Genes and Metabolites in Response to Carbon Starvation

(A) KEGG pathway enrichment analysis of significantly changing metabolites (measured by untargeted metabolomics) between starvation and growth conditions in WT and ppGpp^0 strains. Pathways are displayed if the enrichment p-value (FDR adjusted with Benjamini-Hochberg procedure) is < 0.01 in at least one condition; black, n.s. (not significant). Pathways changing in a (p)ppGpp-dependent manner during starvation are marked in red. m., metabolism; b., biosynthesis; d., degradation.

(B) Clustergram of metabolite fold changes between starvation and growth conditions in WT and ppGpp^0 strains as quantified by targeted metabolomics analysis.

(C and D) Metabolite and RNA-seq fold changes between starvation and growth conditions for WT (C) and ppGpp^0 (D) projected on the metabolic subnetwork defined in Figure 3F. 3P-glycerate, 3-phosphoglycerate; BP-glycerate, bisphosphoglycerate; b., biosynthesis; DHAP, dihydroxyacetone phosphate; F1P, fructose-1-phospate; F6P, fructose-6-phospate; FBP, fructose-bisphosphate; G1P, glucose-1-phospate; G6P, glucose-6-phospate; GABA, gamma-aminobutyric acid; m., metabolism; PEP, phosphoenolpyruvate; S7P, sedoheptulose 7-phosphate. See also Figure S3, Table S5.

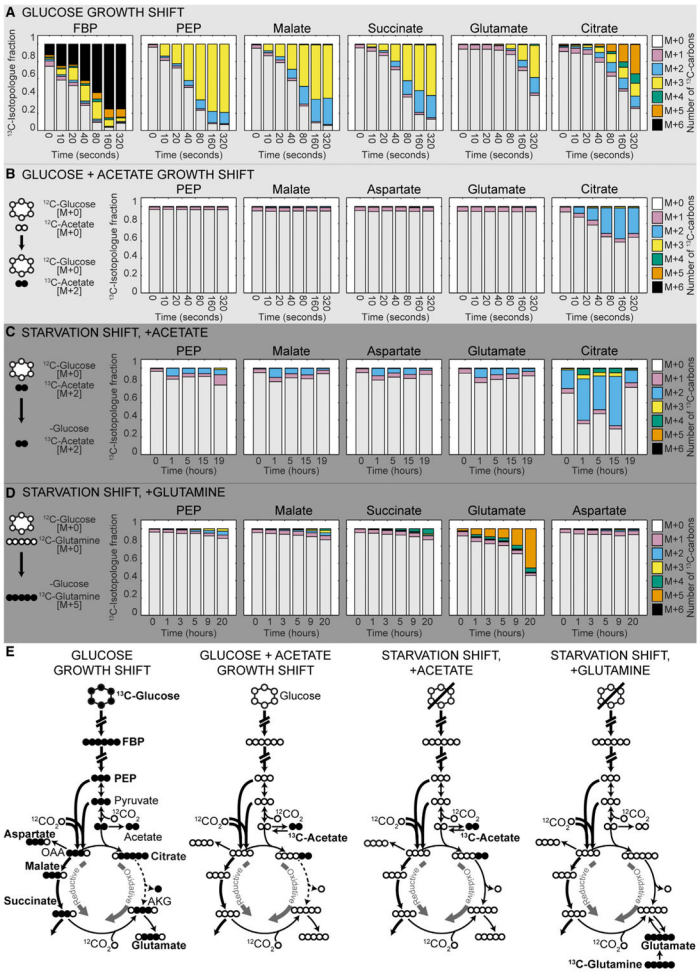

Figure 5. *B. thetaiotaomicron* Produces Alpha-Ketoglutarate through the Reductive Branch of the TCA Cycle during Growth and Starvation

(A–D) Labeled isotopologue fractions of metabolites collected from *B. thetaiotaomicron* cultures shifted from (A) unlabeled glucose to [U-^{13}C] glucose; (B) unlabeled glucose and acetate to unlabeled glucose and [U-^{13}C] acetate; (C) unlabeled glucose and [U-^{13}C] acetate to [U-^{13}C] acetate; (D) unlabeled glucose and glutamine to [U-^{13}C] glutamine. [M + X] indicates the number of ^{13}C-labeled carbon atoms in an isotopologue of a metabolite (maximal value of X is the number of carbons in the molecule). ^{13}C isotopologue fractions reflect the proportions of differently labeled isotopologues in the total pool of a metabolite. (E) Schematic representation of label propagation observed in each shift experiment and underlying metabolic fluxes. AKG, alpha-ketoglutarate; FBP, fructose-bisphosphate; OAA, oxaloacetate; PEP, phosphoenolpyruvate. [M + X] indicates mass isotopologue with X ^{13}C atoms.

See also Figure S4, Table S6.

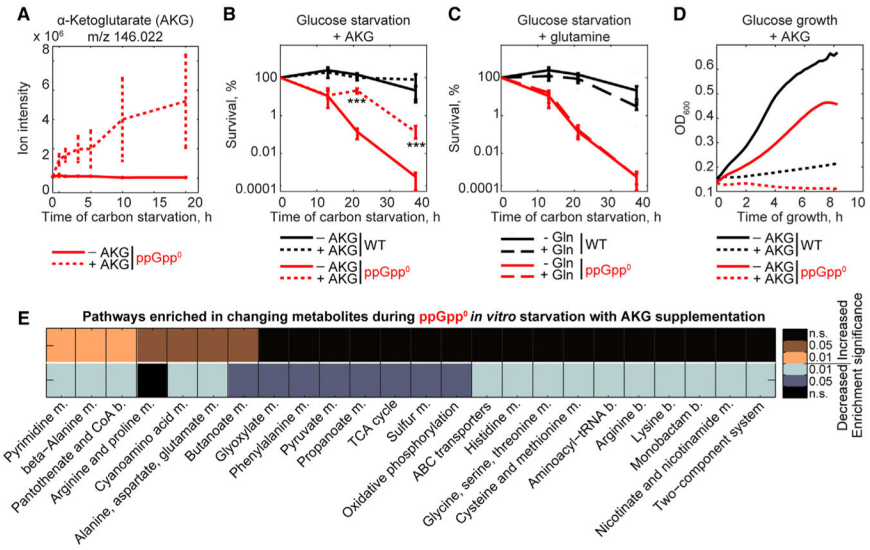

Figure 6. Alpha-Ketoglutarate (AKG) Is Sufficient to Promote ppGpp^0 Survival and Partially Restore Its Metabolic Phenotype during Carbon Starvation

(A) AKG levels in the ppGpp^0 mutant during carbon starvation with and without dimethyl-AKG supplementation. Error bars represent standard deviation of three biological replicates.

(B and C) Survival of WT and ppGpp^0 strains during carbon starvation with and without dimethyl-AKG (B) or glutamine (C). Error bars represent standard deviation of three biological replicates. Significant differences between survival of a given strain with and without supplementation are indicated with asterisks (***$p < 0.001$, Tukey's HSD test and FDR adjustment with Benjamini-Hochberg procedure).

(D) Growth curves of WT and ppGpp^0 strains in glucose minimal medium with and without dimethyl-AKG.

(E) KEGG pathway enrichment analysis for increasing (orange) and decreasing (blue) metabolites in the *B. thetaiotaomicron* ppGpp^0 strain during carbon starvation with dimethyl-AKG versus no dimethyl-AKG supplementation. Pathways are displayed if the enrichment p-value (FDR adjusted with Benjamini-Hochberg procedure) is < 0.1 in at least one condition; black, n.s. (not significant). m., metabolism, b., biosynthesis.

See also Figure S5, Table S7.